 doi:10.20944/preprints202103.0550.v1

Article

Graphene oxide topical administration: skin permeability studies

Filipa A. L. S. Silva[1,2], Raquel Costa-Almeida[1,2], Licínia Timochenco[3], Sara I. Amaral[1,2,3], Soraia Pinto[1,2,4], Inês C. Gonçalves[1,2], José R. Fernandes[5,6], Fernão D. Magalhães[3], Bruno Sarmento[1,2,7], Artur M. Pinto[1,2,3*]

1 i3S—Instituto de Investigação e Inovação em Saúde, Universidade do Porto, Rua Alfredo Allen, 208, Porto 4200-180, Portugal;
2 INEB—Instituto de Engenharia Biomédica, Universidade do Porto, Rua Alfredo Allen, 208, Porto 4200-180, Portugal;
3 LEPABE—Laboratory for Process Engineering, Environment, Biotechnology and Energy, Faculdade de Engenharia, Universidade do Porto, Porto 4200-180, Portugal;
4 ICBAS – Instituto de Ciências Biomédicas Abel Salazar, Universidade do Porto, Rua Jorge Viterbo Ferreira, 228, Porto 4050-313, Portugal;
5 CQVR – Centro de Química Vila Real, Universidade de Trás-os-Montes e Alto Douro, Portugal;
6 Physical Department, University of Trás-os-Montes and Alto Douro, Quinta de Prados, 5001-801, Vila Real, Portugal
7 CESPU, IINFACTS – Institute for Research and Advanced Training in Health Sciences and Technologies, Rua Central de Gandra 1317, Gandra, 4585-116, Portugal.
* Correspondence: arturp@fe.up.pt.

Abstract: Nanostructured carriers have been widely used in pharmaceutical formulations for dermatological treatment. They offer targeted drug delivery, sustained release, improved biostability, and low toxicity, usually presenting advantages over conventional formulations. Due to its large surface area, small size and photothermal properties, graphene oxide (GO) has the potential to be used for such applications. Nanographene oxide (GOn) presented average sizes of 197.6 ± 11.8 nm, and a surface charge of -39.4 ± 1.8 mV, being stable in water for over 6 months. 55.5 % of the mass of GOn dispersion (at a concentration of 1 mg mL^{-1}) permeated the skin after 6 h of exposure. GOn dispersions have been shown to absorb near-infrared radiation, reaching temperatures up to 45.7 °C, within mild photothermal therapy temperature range. Furthermore, GOn in amounts superior to those which could permeate the skin were shown not to affect human skin fibroblasts (HFF-1) morphology or viability, after 24 h of incubation. Due to its large size, no skin permeation was observed for graphite particles in aqueous dispersions stabilized with Pluronic P-123 (Gt-P-123). Altogether, for the first time, GOn potential as a topic administration agent and for delivery of photothermal therapy has been demonstrated.

Keywords: biocompatibility; carbon nanomaterials; graphite; phototherapy; skin disease.

1. Introduction

Skin diseases are one of the leading causes of global disease burden, affecting millions of people worldwide. In the United States of America (USA), nearly 85 million people are seen by a physician for at least 1 skin disease every year. This leads to an estimated direct health care cost of $75 billion and an indirect lost opportunity cost of $11 billion. Further, mortality was noted in half of the 24 skin disease categories. The costs and prevalence of skin disease are comparable with or exceed other diseases with significant public health concerns, such as cardiovascular disease and diabetes. Chronic and incurable skin diseases, such as psoriasis, atopic dermatitis (AD), and vitiligo are associated with physical discomfort and impairment of patients' quality of life; whereas malignant diseases,

Preprints (www.preprints.org) | NOT PEER-REVIEWED | Posted: 22 March 2021 doi:10.20944/preprints202103.0550.v1

such as, basal cell carcinoma if not early and properly treated can lead to mortality. Therefore, new and more effective treatment strategies are needed to deal with skin disease. [1,2]

Guidelines for treatment of Psoriasis, AD, and Vitiligo include as first or second line options phototherapy with ultraviolet radiation combined or not with drugs (*e.g.*, psoralen), while for Basal Cell Carcinoma (BCC), photodynamic therapy (PDT) with photosensitizers, such as 5-aminolevulinic acid (5-ALA) activated by near-infrared (NIR) radiation are listed in the first line of treatments. [3-6] This therapy has also been reported in literature for the abovementioned diseases. [7] However, such treatments still present limitations due to the low stability, toxicity, and skin penetration of commonly used drugs. [8]

Nanostructured carriers are an upcoming option for drug delivery because of their advantages over conventional formulations. Nanoparticles can penetrate skin depending on size, charge, and surface chemistry. These colloidal particulate systems with sizes often around or below 200 nm offer targeted drug delivery, sustained release, improved biostability, and low toxicity. Nanoparticles are observed to penetrate skin intracellularly, intercellularly, or via hair follicles. Many nanocarriers such as polymeric, inorganic and lipid nanoparticles have been developed, and some like carbon based nanomaterials still need further exploration for future use in dermatological applications. [9,10]

Carbon materials have been generally reported to have strong light absorption while maintaining their stability, therefore, being a promising new class of agents for phototherapy. Furthermore, such materials skin biocompatibility has been observed since ancient times, where manmade permanent tattoos using pulverized charcoal could be placed under the skin without apparent adverse effects. [11]

A more recent type of carbon materials, graphene-based materials (GBM), have been widely explored as promising drug delivery vehicles. The large specific surface area of GBM facilitates efficient loading of drugs via surface adsorption or chemical functionalization. Graphene-based nanosystems have been shown to improve the stability, bioavailability, and photodynamic efficiency of organic photosensitizer molecules. They have also been shown to behave as electron sinks for enhanced visible light photodynamic activities. Owing to its intrinsic near infrared absorption properties, GBM can be designed to combine both photodynamic and photothermal hyperthermia for optimum therapeutic efficiency. Comparing with other nanocarriers, GBM possess much higher drug loading capacity and radiation absorbance. It has been shown that GBM can be targeted to specific cells, for delivery of photosensitizers in PDT. [12-17] Furthermore, GBM are similar to active substances used in the treatment of dermatological conditions, such as Psoriasis (*e.g.*, anthracene, anthralin, psoralen, coal tar), which perspectives high potential for phototherapeutic effect using GBM themselves and good affinity with the drugs to be delivered. GBM have been shown to be biocompatible up to high concentrations that hardly will be achieved in dermatological phototherapy. [18-20] Moreover, some GBM have been reported to be biodegradable by human enzymes. [21,22] For those reasons, the use of GBM can be regarded as promising option for target applications.

Graphene is the elementary structure of graphite and is composed by a single layer of sp^2 hybridized carbon atoms organized in a hexagonal crystalline structure, forming a two-dimensional sheet. This material possesses high surface area, mechanical strength and thermal and electrical conductivity that supports its application in fields as diverse as energy technology, nanoelectronics, composite materials, and sensors. [23-31] In addition, graphene also possesses good optical transparency (97.7 %) and high extinction coefficient in the NIR range, responsible for its high photothermal conversion ability. [32]

The application of graphene in biomedical area is limited by its hydrophobicity, which can be surpassed by its oxidation and consequent introduction of oxygen-containing functional groups, such as carboxyl, hydroxyl and epoxide groups. [33] Graphene oxide (GO) is similar to graphene, but the presence of these polar and reactive groups allows surface functionalization and coupling with other molecules such as chemotherapeutic drugs or photosensitizers that make possible its utilization as drug carriers. Thus, several

Preprints (www.preprints.org) | NOT PEER-REVIEWED | Posted: 22 March 2021 doi:10.20944/preprints202103.0550.v1

biomedical applications of GO have also been studied, including biosensing/bioimaging, drug delivery, antibacterial or cancer photothermal therapy. [34-39]

Beyond the polarity, the materials' size is of key importance in biomedicine. Considering that biological systems as membranes and protein complexes are natural nanostructures, the utilization of nanomaterials has a clear advantage in the interaction with these structures, making possible cellular uptake, penetration into blood vessels and renal clearance. [40] Thus, the successful application of GO in biomedical field require size reduction to nanoscale.

The administration of nano graphene oxide (GOn) in *in vivo* models to test the efficacy of these material as platforms for cancer or infections treatment, is generally done by intravenous or intratumoral injection. [41-45] However, these approaches present some disadvantages, once they are invasive procedures, more susceptible to trigger adverse local reactions. [46,47] Thus, the topical application of GOn to treat skin diseases, including skin cancer, local infections or other diseases for which the treatment can be delivered through this route, is positioned as an interesting approach, since it is a non-invasive procedure that allows a localized material distribution, preventing any systemic side effects. [46-50]

In view of these aspects, for the first time, since to our knowledge, we determined the permeability of single layer GO with nanometric lateral dimensions (GOn) and micrometric graphite stabilized with Pluronic P-123 (Gt-P-123) water dispersions through human skin. The influence of lateral dimensions and exfoliation procedure in skin permeation were also discussed. Finally, the biocompatibility of GOn nanosheets was evaluated using human skin fibroblasts (HFF-1 cell line).

2. Materials and Methods

2.1. Graphite dispersions preparation

Graphite powder (size ≤ 20 μm, Sigma Aldrich, Missouri, EUA) dispersions were stabilized by Pluronic P-123 (Sigma Aldrich, Missouri, EUA). Graphite powder (Gt) and Pluronic P-123 (P-123) at final concentrations of 1 mg mL^{-1} and 0.5 % (w/w), respectively, were dispersed in deionized water and then sonicated for 10 minutes using an ultrasonic bath (ATM40-3LCD, Ovan, Barcelona, Spain) to obtain stable dispersions.

2.2. GOn dispersions production

Graphite oxide (GtO) was produced by Gt oxidation (size ≤ 20 μm, Sigma Aldrich, Missouri, EUA) using the modified Hummers method, as described elsewhere. [18,51] Briefly, 4 g of graphite was added to a mixture of 40 mL of phosphoric acid (H_3PO_4, Chem-Lab, Zedelgem, Belgium) and 160 mL of sulfuric acid (H_2SO_4, VWR, Frankfurt, Germany) under stirring, and cooled using an ice bath. Then, 24 g of potassium permanganate ($KMnO_4$, JMGS, Odivelas, Portugal) were added gently under stirring. Subsequently, 600 mL of H_2O was slowly added, controlling temperature using an ice bath. Finally, hydrogen peroxide (H_2O_2, 26.5 mL, Frankfurt, VWR, Germany) was added and the mixture was left to rest overnight. Afterwards, the solution was decanted to separate the solid phase from the acidic solution, centrifuged at 4000 rpm during 20 minutes and redispersed in distilled water. The process was repeated until water pH was achieved in the supernatant. The pellet was recovered, redispersed in distilled water and sonicated during 8 h using a high-power ultrasonic probe (UIP1000hd, Hielscher Ultrasonics GmbH, Teltow, German) to simultaneously exfoliate GtO and breakup the sheets to lateral sizes close to a hundred nanometers, yielding the final product, nanographene oxide (GOn) at a concentration of 7 mg mL^{-1}, which has been further diluted for testing.

2.3 Characterization

Preprints (www.preprints.org) | NOT PEER-REVIEWED | Posted: 22 March 2021 doi:10.20944/preprints202103.0550.v1

2.3.1 Optical microscopy

Gt-P-123 dispersions at a Gt concentration of 1 mg mL^{-1} were placed in a 48-well cell culture plate (500 µL) and observed under an inverted optical microscope (CKX41, Olympus, Tokyo, Japan) coupled with a digital camera (SC30, Olympus, Tokyo, Japan).

2.3.2 Transmission electron microscopy

Morphology of GOn particles was analyzed by transmission electron microscopy (TEM, JEOL JEM 1400 TEM, Tokyo, Japan). Aqueous dispersions at a concentration of 50 µg mL^{-1} were deposited on a carbon coated TEM grid (10 µL) and allowed to deposit for 1 minute. The excess material was removed by capillarity using filter paper.

2.3.3 Dynamic Light Scattering and Zeta potential measurements

GOn particles size and zeta potential were determined by dynamic light scattering (DLS) and electrophoretic light scattering (ELS), respectively, using a Zetasizer Nano-ZS (Malvern Instruments, Malvern, UK). GOn was analyzed in a disposable Zetasizer cuvette (Malvern Instruments, Malvern, UK) at a concentration of 25 µg mL^{-1} and pH 6. Each measurement was performed in triplicate at room temperature and results are reported as mean and standard deviation.

2.3.4 Ultraviolet-visible spectroscopy

Absorption spectra of GOn, G-P-123, and P-123 (only) were acquired using a Lambda 35 UV/Vis spectrometer (Perkin-Elmer, Massachusetts, USA). Samples were prepared at a concentration of 25 µg mL^{-1} and transferred to a 50 µL quartz cuvette (Hellma Analytics, Müllheim, Germany) with 10 mm light path length and spectra were recorded in the range of 200 – 850 nm. Measurements were performed at room temperature with baseline correction based on water as a blank control.

2.4 Skin permeation experiments

2.4.1 Human samples

Human skin with 0.8 mm thickness were obtained from abdominal surgery of one healthy woman (Department of Plastic Surgery, São João Hospital, Porto, Portugal). The experimental protocol was approved by the Bioethics Committee of the São João Hospital and written informed consent form was provided to the volunteer. The skin was washed with ultrapure water, and the hair and subcutaneous fatty tissue were removed with scissors. The skin was stored at -20 °C wrapped in aluminum foil until further use.

2.4.2 Skin permeation assays

Human skin permeability to Gt-P-123 and GOn was evaluated using Franz diffusion cells with 9 mm clear jacketed with flat ground joint, 5 mL receptor volume and permeation area of 0.785 cm^2 (PermeGear, Inc., Pennsylvania, USA).

The skin previously prepared was mounted in the Franz cells with *stratum corneum* (SC) towards the donor chamber. The receptor compartment was filled with phosphate buffer 0.1 M at pH 7.4 (PBS) maintained at 37 °C and continuously stirred at 300 rpm, to ensure sink conditions. Then, 500 µL of Gt or GOn dispersions at a concentration of 1 mg mL^{-1} were placed in the donor chamber and sealed with paraffin film to provide occlusive conditions. After 1, 2, 3, 4, 5 and 6 h, an aliquot of the receptor medium (100 µL) was collected to determine by absorbance the amount of compound that permeated through the skin. The same volume of PBS was readded to the receptor compartment. A calibration

Preprints (www.preprints.org) | NOT PEER-REVIEWED | Posted: 22 March 2021 doi:10.20944/preprints202103.0550.v1

curve for both materials was prepared to extrapolate Gt-P-123 or GOn concentrations at the receptor compartment. Materials permeated mass was obtained by mutiplying the sample concentration for the volume of receptor compartment. Results are presented as cumulative mass and percentage of material that permeated through the skin. All assays were performed in triplicate.

2.5 GOn photothermal therapy potential

2.5.1 Near infrared irradiation

In order to evaluate the light-to-heat conversion ability of GOn, 500 µL of the dispersion at a concentration of 1 mg mL^{-1} was placed in a 48-well cell culture plate. Wells with water only were used as a control. Samples were irradiated using a LED based source with a peak emission around 810 nm (NIR region) and irradiance of 150 mW cm^{-2}. [52] The light-induced temperature increment on the samples was monitored during 30 minutes using a type K thermocouple (Hanna instruments, Póvoa de Varzim, Portugal) placed centered and half-height in the suspension. Assays were performed in 3 different experiments, with 3 replicates for condition, and results are presented as mean and standard deviation of absolute temperature.

2.6 In vitro studies

2.6.1 Cell culture

Biological studies were performed using HFF-1 human skin fibroblast cells (SCRC-1041, ATCC, Virginia, USA). Cells were cultured in Dulbecco's Modified Eagle's Medium (DMEM, ATCC Virginia, USA) supplemented with 10 % (v/v) fetal bovine serum (Alfagene, Lisbon, Portugal) and 1 % (v/v) penicillin/streptomycin (Biowest, Nuaillé, France). Cells were maintained in a humidified atmosphere with 5 % CO_2 at 37 °C.

2.6.2 Resazurin assay

The effect of GOn on cell viability was evaluated using different material amounts (180-300 µg/well, correspondent to 300-500 µg mL^{-1}). Each well has an area of 0.91 cm^2. Cells were seeded in 48-well plates at a density of 1×10^4 cells/well and incubated at 37 °C and 5 % CO_2 for 24 h. After, cell medium was replaced by GOn dispersions in a final volume of 600 µL per well (in complete DMEM) and cells were incubated with the materials for 24 h. Then, cell viability was quantified by resazurin assay. Briefly, material dispersions were removed, cells were washed with PBS and incubated in 10 % (v/v) resazurin reagent (Sigma-Aldrich, Missouri, USA) in cell culture medium at 37 °C and 5 % CO_2 for 2 h. The fluorescence ($\lambda_{ex/em}$ = 530/590 nm) of the supernatant was measured using a micro-plate reader spectrophotometer (Synergy Mx, Bio-Tek Instruments, Vermont, USA). Negative and positive controls for cell viability decrease were performed by HFF-1 incubation with complete DMEM and 10 % (v/v) dimethyl sulfoxide (DMSO) in complete DMEM, respectively. Data for each sample were normalized to the negative control (cells in culture media only) and results are presented as % of the control. All assays were performed in triplicate with six replicates for each condition tested.

2.6.3 Optical microscopy

The effecf of GOn on cells morphology was evaluated by optical microscopy. Cells were seeded and exposed to GOn as described for resazurin assay. After 24 h, cells were washed 3 times with PBS and analysed using an inverted optical microscope (CKX41, Olympus, Tokyo, Japan) coupled with a digital camera (SC30, Olympus, Tokyo, Japan).

Preprints (www.preprints.org) | NOT PEER-REVIEWED | Posted: 22 March 2021 doi:10.20944/preprints202103.0550.v1

3. Results and discussion

3.1 Gt and GOn dispersions physico-chemical characterization

Graphite (Gt) was dispersed by sonication in water, however it precipitated due to its large size (≤ 20 μm) and hydrophobicity. Therefore, it was stabilized with Pluronic P-123 (P-123), a non-ionic surfactant composed of poly(ethylene oxide) and poly(propylene oxide) blocks. [53] Nanosized GO (GOn) was produced by Gt oxidation and exfoliation using a modified Hummers method, followed by high-power ultrasonication. Figure 1 shows Gt, Gt-P-123, and GOn aqueous dispersions at a concentration of 1 mg mL^{-1}.

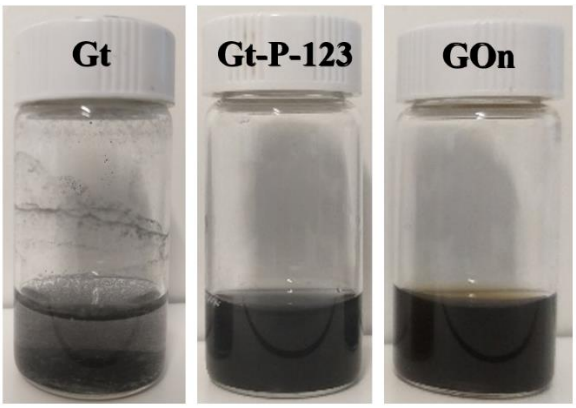

Figure 1. Images of graphite without Pluronic P-123 (Gt), Graphite + Pluronic P-123 (Gt-P-123) and graphene oxide (GOn) dispersions, at a concentration of 1 mg mL^{-1}, in glass vials for stability evaluation. Sedimentation is visible on Gt sample after only a few seconds.

The presence of P-123 at a concentration of 0.5 % (w/v) stabilized Gt in water, allowing to obtain homogenous blackish dispersions without formation of any precipitate. Such dispersions are stable for 12 h, period after which the sedimentation becomes visible. However, it is possible to easily redisperse them by manual shaking. GOn water dispersions presented a typical brownish appearance and good stability. Such dispersions present a shelf-life of at least 6 months (longest observation period tested).

Gt-P-123 water dispersions were observed by optical microscopy (Figure 2), revealing to have small particles with sizes from a few μm, to large agglomerates up to 200 μm.

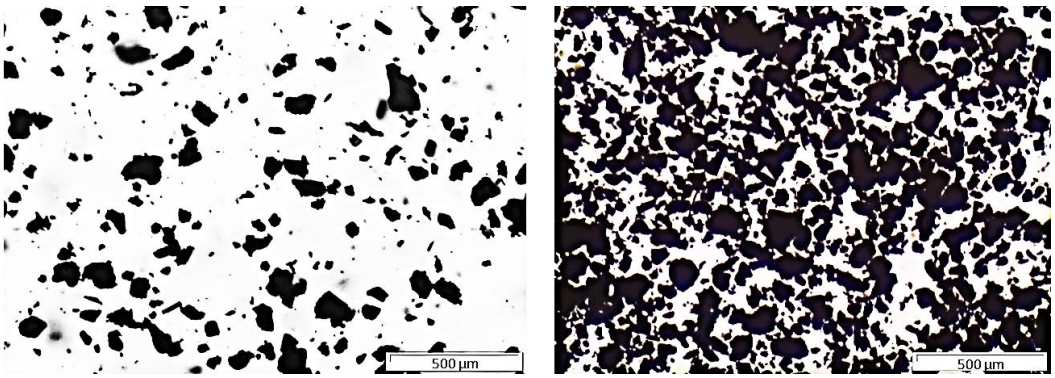

Figure 2. Representative optical microscopy images of Graphite-P123 dispersions (1 mg mL^{-1}). Scale bar represents 500 μm.

The morphology of GOn nanosheets was observed by TEM. Figure 3 shows that our high-power sonication size reduction method, allow achieving well exfoliated GOn single layer particles with sizes below 200 nm.

Preprints (www.preprints.org) | NOT PEER-REVIEWED | Posted: 22 March 2021 doi:10.20944/preprints202103.0550.v1

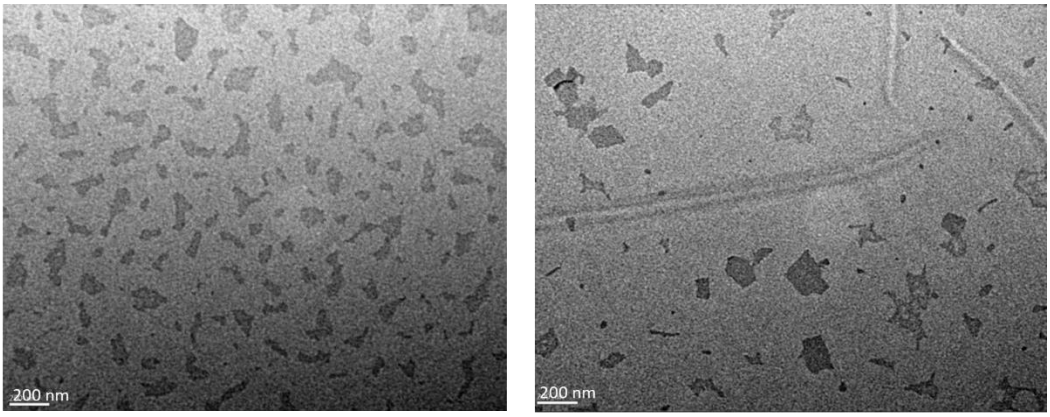

Figure 3. Representative TEM images of GOn aqueous dispersions (50 μg mL^{-1}). Scale bar represents 200 nm.

Table 1 shows particle size and surface charge of GOn measured using a Zetasizer by DLS and ELS, respectively. Gt-P-123 dispersions presented a particle size too large to be analyzed using a Zetasizer, however, it has already been clearly observed in optical microscopy images (Figure 2), furthermore, this is a commercial material whose particle size is already described. Particle size values determined by DLS for GOn are consistent with TEM measurements. GOn presented hydrodynamic diameters of 197.6 ± 11.8 nm. The surface charge was -39.4 ± 1.8 mV, which is a high value that explains the excellent aqueous dispersion stability visually observed for more than 6 months for this material. [54]

Table 1. Surface charge of GOn aqueous dispersions diluted at a concentration of 25 μg mL^{-1} and pH 6 (n = 3).

Material	Size (nm)	Surface charge (mV)
GOn	197.6 ± 11.8	-39.4 ± 1.8

The absorbance spectra of GOn, Gt-P-123, and P-123 were determined by UV/Visible spectroscopy (Figure 4). GOn spectra presented an absorbance peak at λ_{max} = 230 nm, attributed to $\pi - \pi^*$ electronic transitions in sp^2 clusters, and a shoulder peak at 300 nm, corresponding to $n - \pi^*$ transitions of free electron pairs in oxygen atoms in C=O bonds from carboxyl and carbonyl groups. [55] Gt-P-123, presented a typical spectrum for graphitic materials, with peaks at 223 and 273 nm. [56] Residual absorbance was detected for Pluronic-only when at the same concentration used to stabilize Gt in water.

Preprints (www.preprints.org) | NOT PEER-REVIEWED | Posted: 22 March 2021 doi:10.20944/preprints202103.0550.v1

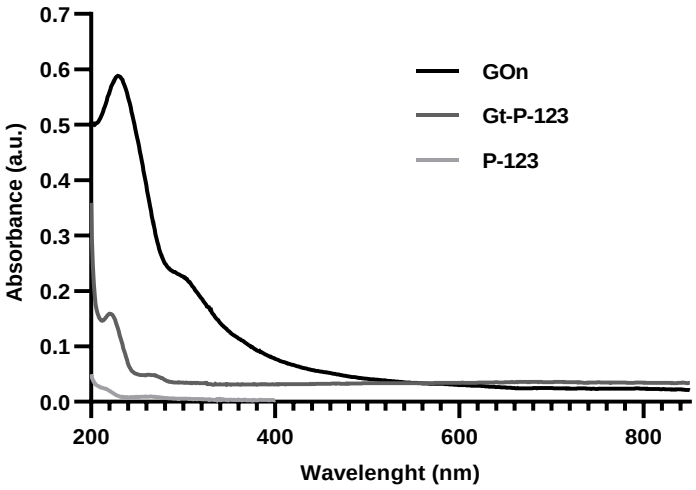

Figure 4. UV/Visible absorption spectra for water dispersions of nanographene oxide (GOn), graphite stabilized with Pluronic P-123 (Gt-P-123), and Pluronic P-123 only (P-123) (at the same concentration used to stabilize Gt).

3.2 Skin permeability of GOn and Gt-P-123

The permeation through human skin of GOn and Gt-P-123 was evaluated immobilizing the skin samples between the donor and receiver compartments of Franz cells (Figure 5A). The donor compartment was filled with 500 μL of GOn or Gt-P-123, at a concentration of 1 mg mL^{-1}. Samples were collected from the receptor compartment every hour, during 6 h. The amount of material that permeated the skin was quantified by UV/Visible spectroscopy. GOn and Gt-P-123 concentrations were determined from absorbance values at wavelengths correspondent to the maximum absorption peaks in their spectra (230 nm for GOn and 223 nm for Gt-P-123). This was performed by matching the absorption values obtained with calibration curves performed with a range of known concentrations of both materials.

Preprints (www.preprints.org) | NOT PEER-REVIEWED | Posted: 22 March 2021 doi:10.20944/preprints202103.0550.v1

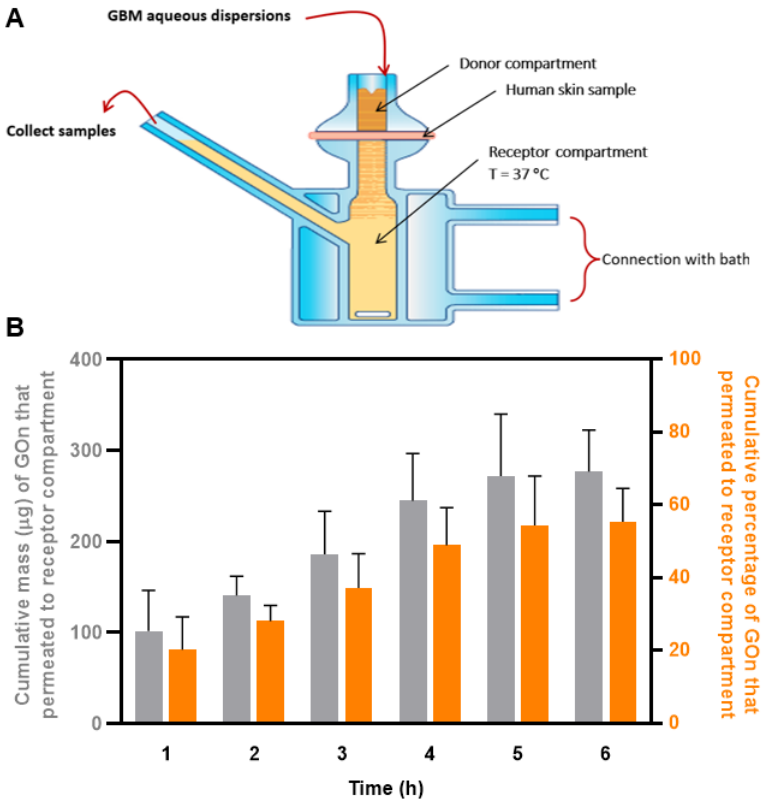

Figure 5. Skin permeation studies for GOn. A) Schematic representation of the skin permeability experimental setup using a Franz cells system. B) Cumulative GOn mass in absolute value (µg) and in percentage that permeated from donor to receptor compartment. Results are presented as average and standard deviation.

Gt-P-123 was not detected in the receptor compartment even after 6 h, indicating that it cannot permeate through the skin sample. This reaffirms the relevance of reaching nanometric size to achieve and maximize skin permeation of nanoparticles. [57] This material has therefore no use as a possible vehicle for drug delivery or phototherapy in skin diseases, and was not further characterized.

Results for GOn skin permeation are presented in Figure 5B. GOn was capable of permeating across the skin in a time-dependent manner. It is relevant to notice that besides presenting a lateral size below 200 nm, GOn is formed by a single layer of carbon atoms, therefore presenting a very low thickness and high flexibility, which facilitates transport through skin. On the other hand, Gt is composed by numerous stacked graphene layers. After 1 h, the percentage of GOn that permeated from donor to receptor compartment was 20.3 % corresponding to a mean permeated mass of 101.4 µg. While, after 2 h the percentage of GOn that permeated through the skin increased to 28.7 %, corresponding to a mean permeated mass of 140.5 µg. After 4 h, 49 % of the GOn placed in the donor compartment crossed to the receptor compartment. The amount of material that permeated through skin at 5 h increased by approximately 5.4 % (271.7 µg) when compared to 4 h, whereas from 5 to 6 h the increase was only of around 1 %. For this reason, the assay was stopped at this point. The total mass that permeated the skin was of 276.7 µg, corresponding to 55.5 % of the material originally present. Considering the results, there are few advantages in prolonging an eventual topic administration of GOn for longer than 4 h, when approximately half of the material (244.9 µg) crossed the skin. Coincidently, phototherapy treatments for skin disease involves topical administration of pharmaceutical formulation usually 4 h before skin irradiation. [7,58]

3.2 GOn photothermal therapy potential

Preprints (www.preprints.org) | NOT PEER-REVIEWED | Posted: 22 March 2021 doi:10.20944/preprints202103.0550.v1

Since GOn particles ability to permeate through human skin has been demonstrated, they might have potential to be used in dermatological applications, such as photothermal therapy of skin cancer. [13-16,59] For that reason, the ability of GOn to convert NIR light into thermal energy was evaluated (Figure 6). GOn dispersions reached temperatures of 40.3 °C and 45.7 °C, after 15 and 30 minutes of NIR irradiation, respectively. These values corresponded to an increment of 10 °C in relation to water only (control). Therefore, GOn dispersions confirmed to be effective agents to induce a temperature increase within mild photothermal therapy temperature range, which has been reported to induce death of skin cancer cells. [59]

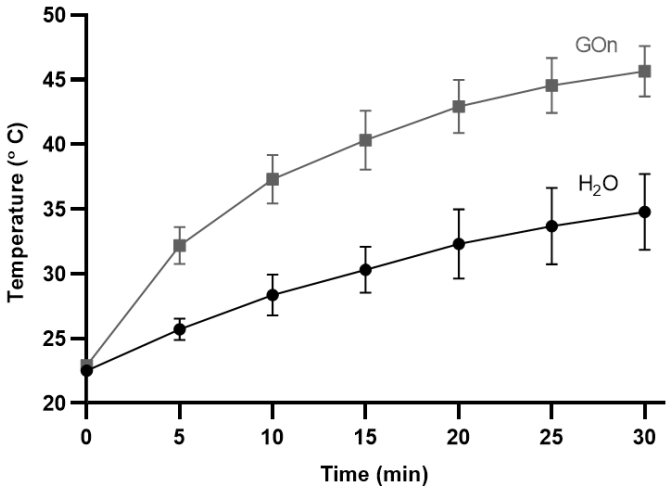

Figure 6. Photothermal heating curves of water-only or GOn aqueous dispersions at a concentration of 1 mg mL^{-1}.

3.3 In vitro biocompatibility of GOn

Since GOn has the potential to be used for applications such as skin cancer phototherapy and topic drug delivery [13-16,59,60], it is important to assure that the used particles are non-toxic towards healthy skin cells. For that reason, human foreskin fibroblasts (HFF-1) were incubated with increasing concentrations (300-500 µg mL^{-1}) of GOn during 24 h, and cell viability assessed through the resazurin assay (Figure 7).

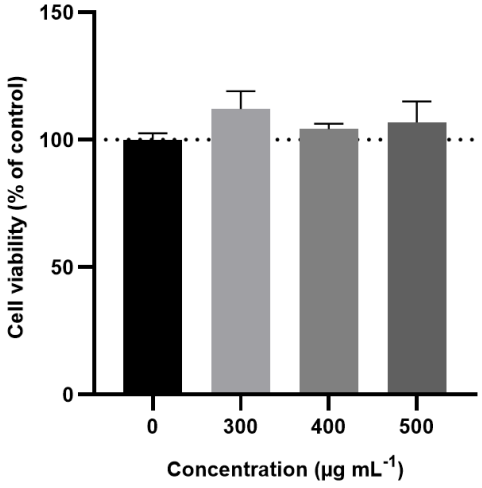

Figure 7. Cellular viability of HFF-1 cells determined using the resazurin assay. Results are normalized with respect to values of the control without material (cell culture media only), and presented as average and standard deviation.

Preprints (www.preprints.org) | NOT PEER-REVIEWED | Posted: 22 March 2021 doi:10.20944/preprints202103.0550.v1

It is relevant to mention that unlike what happens with HFF-1 exposed to the full amount of material placed in the wells during 24 h, in skin permeation tests, the particles go through the skin in a period up to only 6 h. Therefore, the time of exposure and GOn amounts inside the skin are lower during permeation, than in the *in vitro* biological tests presented in this section. Even though, GOn did not induce any decrease in HFF-1 cell viability, for all conditions tested, as compared to the control condition in which the cells were incubated in cell culture media without materials. Furthermore, HFF-1 cells presented a normal spindle like shape (Figure 8), characteristic of human skin fibroblasts, when exposed or not to GOn. This reaffirms the potential of the nanosized single layer GOn herein reported to be used in the biomedical field, in applications such as, for example, skin cancer phototherapy or topic drug delivery. [13-16,59,60]

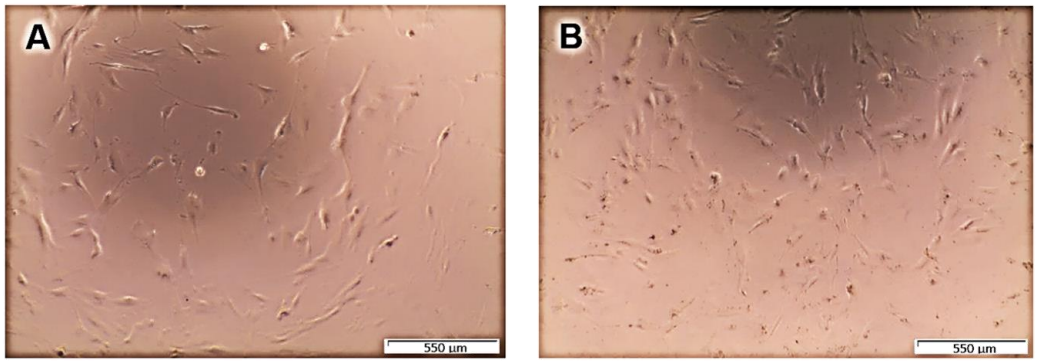

Figure 8. Representative optical microscopy images of HFF-1 cells in cell culture media only (A) and after 24 h of contact with 300 µg of GOn (B). Scale bar represents 550 µm.

4. Conclusions

In order to evaluate their potential for dermatological applications, two different carbon materials were studied in terms of physico-chemical characteristics and human skin permeation. Graphite particles in aqueous dispersions stabilized with Pluronic P-123 (Gt-P-123) presented sizes between a few to hundreds (agglomerates) of microns. The presence of P-123 at a concentration of 0.5 % (w/v) stabilized Gt in water, allowing to obtain homogenous blackish dispersions without sedimentation. Such dispersions are stable for 12 h, period after which they precipitate. However, they can be easily redispersed. Gt-P-123 presented a typical spectrum for graphitic materials, with peaks at 223 and 273 nm. Due its large size, no skin permeation was observed for Gt-P-123.

Nanographene oxide (GOn) particles presented average lateral sizes of 197.6 ± 11.8 nm, and a surface charge of -39.4 ± 1.8 mV, being stable in water dispersion for up to 6 months. GOn spectra presented an absorbance peak at λ_{max} = 230 nm, attributed to $\pi - \pi^*$ electronic transitions in sp^2 clusters, and a shoulder peak at 300 nm, corresponding to $n - \pi^*$ transitions of free electron pairs in oxygen atoms in C=O bonds from carboxyl and carbonyl groups.

GOn was capable of permeating across skin in a time-dependent manner. 20.3% of the mass of GOn (1 mg mL^{-1}) put in contact with the skin sample permeated after 1 h, while 55.5 % permeated after 6 h. Furthermore, GOn dispersions were shown to absorb near-infrared radiation, causing local temperature to reach up to 45.7 °C, within mild photothermal therapy temperature range.

Finally, GOn in amounts superior to those which could permeate the skin were show not to affect human skin fibroblast (HFF-1) morphology or viability, after 24 h of incubation.

GOn potential as a topic administration agent and for delivery of photothermal therapy has been demonstrated. This material can also be considered as a drug delivery vehicle for drugs used in skin disease, potentially improving drugs' stability and penetration,

allowing for reduced therapeutic doses and avoiding side effects of systemic therapy and high topical doses.

Author Contributions: Conceptualization, F.A.L.S.S., R.C.-A., F.D.M., and A.M.P.; Methodology, F.A.L.S.S., R.C.-A., L.T., S.I.A, S.P., J.R.F., F.D.M., B.S., and A.M.P.; Validation, F.A.L.S.S., R.C.-A., B.S., F.D.M., and A.M.P; Formal analysis, F.A.L.S.S., R.C.-A., S.I.A., F.D.M, and A.M.P.; Investigation, F.A.L.S.S., R.C.-A., L.T., S.I.A, and S.P.; Resources, J.R.F., I.C.G., F.D.M., B.S., and A.M.P.; Data curation, F.A.L.S.S., R.C.-A., S.I.A, and A.M.P.; Writing—original draft preparation, F.A.L.S.S., R.C-A., and A.M.P.; Writing—review and editing, R.C.-A., L.T, S.I.A, S.P, I.C.G., J.R.F., F.D.M., B.S., and A.M.P.; Supervision, R.C.-A., I.C.G, B.S., F.D.M., and A.M.P.; Project administration, F.D.M., and A.M.P.; Funding acquisition, B.S., I.C.G, F.D.M., and A.M.P. All authors have read and agreed to the published version of the manuscript.

Funding: This work was financed by FEDER funds through the COMPETE 2020 – Operacional Programme for Competitiveness and Internationalisation (POCI), Portugal 2020, and by national funds (PIDDAC) through FCT/MCTES in the framework of the project POCI-01-0145-FEDER-031143, and Base Funding - UIDB/00511/2020 of the Laboratory for Process Engineering, Environment, Biotechnology and Energy – LEPABE. Additional funding included FCT/MCTES in the framework of the project "Institute for Research and Innovation in Health Sciences" (UID/BIM/04293/2019). Authors would also like to thank the support of i3S Scientific Platforms and respective funding: HEMS, member of the national infrastructure PPBI – Portuguese Platform of Bioimaging: POCI-01-0145-FEDER-022122; and Biointerfaces and Nanotechnology (BN) Laboratory, Portuguese Funds through FCT, UID/BIM/04293/2019. Artur Pinto thanks the Portuguese Foundation for Science and Technology (FCT) for the financial support of his work contract through the Scientific Employment Stimulus - Individual Call – [CEECIND/03908/2017]. Soraia Pinto (SFRH/BD/144719/2019) would like to thank to FCT, Portugal for financial support.

Informed Consent Statement: The experimental protocol for the utilization of skin samples was approved by the Bioethics Committee of the São João Hospital and written informed consent form was provided to the volunteer.

Data Availability Statement: The data presented in this study are available on request from the corresponding author.

Acknowledgments: Authors would like to acknowledge the Department of Plastic Surgery, São João Hospital, Porto, Portugal, for providing the human skin samples used, under the collaborative protocol in place between them and i3S.

Conflicts of Interest: The authors declare no conflict of interest.

References

1. Lim, H.W.; Collins, S.A.B.; Resneck, J.S.; Bolognia, J.L.; Hodge, J.A.; Rohrer, T.A.; Van Beek, M.J.; Margolis, D.J.; Sober, A.J.; Weinstock, M.A.; et al. The burden of skin disease in the United States. *J Am Acad Dermatol* **2017**, *76*, 958-+, doi:10.1016/j.jaad.2016.12.043.
2. Laughter, M.R.; Maymone, M.B.C.; Karimkhani, C.; Rundle, C.; Hu, S.; Wolfe, S.; Abuabara, K.; Hollingsworth, P.; Weintraub, G.S.; Dunnick, C.A.; et al. The Burden of Skin and Subcutaneous Diseases in the United States From 1990 to 2017. *Jama Dermatol* **2020**, *156*, 874-881, doi:10.1001/jamadermatol.2020.1573.
3. Eichenfield, L.F.; Tom, W.L.; Chamlin, S.L.; Feldman, S.R.; Hanifin, J.M.; Simpson, E.L.; Berger, T.G.; Bergman, J.N.; Cohen, D.E.; Cooper, K.D.; et al. Guidelines of care for the management of atopic dermatitis Section 1. Diagnosis and assessment of atopic dermatitis. *J Am Acad Dermatol* **2014**, *70*, 338-351, doi:10.1016/j.jaad.2013.10.010.
4. Taieb, A.; Alomar, A.; Boehm, M.; Dell'Anna, M.L.; De Pase, A.; Eleftheriadou, V.; Ezzedine, K.; Gauthier, Y.; Gawkrodger, D.J.; Jouary, T.; et al. Guidelines for the management of vitiligo: the European Dermatology Forum consensus. *Brit J Dermatol* **2013**, *168*, 5-19, doi:10.1111/j.1365-2133.2012.11197.x.
5. Menter, A.; Gottlieb, A.; Feldman, S.R.; Van Voorhees, A.S.; Leonardi, C.L.; Gordon, K.B.; Lebwohl, M.; Koo, J.Y.M.; Elmets, C.A.; Korman, N.J.; et al. Guidelines of care for the management of psoriasis and psoriatic arthritis - Section 1. Overview of

psoriasis and guidelines of care for the treatment of psoriasis with biologics. *J Am Acad Dermatol* **2008**, *58*, 826-850, doi:10.1016/j.jaad.2008.02.039.

6. Bichakjian, C.; Armstrong, A.; Baum, C.; Bordeaux, J.S.; Brown, M.; Busam, K.J.; Eisen, D.B.; Iyengar, V.; Lober, C.; Margolis, D.J.; et al. Guidelines of care for the management of basal cell carcinoma. *J Am Acad Dermatol* **2018**, *78*, 540-559, doi:10.1016/j.jaad.2017.10.006.
7. Ibbotson, S.H. Topical 5-aminolaevulinic acid photodynamic therapy for the treatment of skin conditions other than non-melanoma skin cancer. *Brit J Dermatol* **2002**, *146*, 178-188, doi:DOI 10.1046/j.0007-0963.2001.04689.x.
8. Said, A.; Makki, S.; Muret, P.; Rouland, J.C.; Toubin, G.; Millet, J. Lipophilicity determination of psoralens used in therapy through solubility and partitioning: Comparison of theoretical and experimental approaches. *J Pharm Sci* **1996**, *85*, 387-392, doi:DOI 10.1021/js950367f.
9. Alka Lohani, A.V., Himanshi Joshi, Niti Yadav, and Neha Karki. Nanotechnology-Based Cosmeceuticals. *International Scholarly Research Notices* **2014**, *2014*, doi:https://doi.org/10.1155/2014/843687.
10. Palmer, B.C.; DeLouise, L.A. Nanoparticle-enabled transdermal drug delivery systems for enhanced dose control and tissue targeting. *Molecules* **2016**, *21*, 1719, doi:https://doi.org/10.3390/molecules21121719.
11. A.M. Pinto, P., A. T., Goncalves, I. C. Carbon Biomaterials. In *Biomaterials Science. An Introduction to Materials in Medicine*, 4th ed.; W.R. Wagner, S.-E., S. E., Zhang, G., Yaszemski, M. J. , Ed.; Elsevier: San Diego, California, 2020.
12. Li, Y.; Dong, H.Q.; Li, Y.Y.; Shi, D.L. Graphene-based nanovehicles for photodynamic medical therapy. *Int J Nanomed* **2015**, *10*, 2451-2459, doi:10.2147/Ijn.S68600.
13. Zhang, B.M.; Wang, Y.; Liu, J.Y.; Zhai, G.X. Recent Developments of Phototherapy Based on Graphene Family Nanomaterials. *Curr Med Chem* **2017**, *24*, 268-291, doi:10.2174/0929867323666161019141817.
14. Li, X.; Lovell, J.F.; Yoon, J.; Chen, X. Clinical development and potential of photothermal and photodynamic therapies for cancer. *Nat Rev Clin Oncol* **2020**, *17*, 657-674.
15. Van Straten, D.; Mashayekhi, V.; De Bruijn, H.S.; Oliveira, S.; Robinson, D.J. Oncologic photodynamic therapy: basic principles, current clinical status and future directions. *Cancers* **2017**, *9*, 19.
16. Jiang, B.P.; Zhou, B.; Lin, Z.; Liang, H.; Shen, X.C. Recent advances in carbon nanomaterials for cancer phototherapy. *Chemistry–A European Journal* **2019**, *25*, 3993-4004.
17. Huang, P.; Xu, C.; Lin, J.; Wang, C.; Wang, X.S.; Zhang, C.L.; Zhou, X.J.; Guo, S.W.; Cui, D.X. Folic Acid-conjugated Graphene Oxide loaded with Photosensitizers for Targeting Photodynamic Therapy. *Theranostics* **2011**, *1*, 240-250, doi:10.7150/thno/v01p0240.
18. Pinto, A.M.; Gonçalves, C.; Sousa, D.M.; Ferreira, A.R.; Moreira, J.A.; Gonçalves, I.C.; Magalhaes, F.D.J.C. Smaller particle size and higher oxidation improves biocompatibility of graphene-based materials. *Carbon* **2016**, *99*, 318-329, doi:https://doi.org/10.1016/j.carbon.2015.11.076.
19. Pinto, A.M.; Moreira, J.A.; Magalhaes, F.D.; Goncalves, I.C. Polymer surface adsorption as a strategy to improve the biocompatibility of graphene nanoplatelets. *Colloid Surface B* **2016**, *146*, 818-824, doi:10.1016/j.colsurfb.2016.07.031.
20. Pinto, A.M.; Moreira, S.; Goncalves, I.C.; Gama, F.M.; Mendes, A.M.; Magalhaes, F.D. Biocompatibility of poly(lactic acid) with incorporated graphene-based materials. *Colloid Surface B* **2013**, *104*, 229-238, doi:10.1016/j.colsurfb.2012.12.006.
21. Kurapati, R.; Russier, J.; Squillaci, M.A.; Treossi, E.; Menard-Moyon, C.; Del Rio-Castillo, A.E.; Vazquez, E.; Samori, P.; Palermo, V.; Bianco, A. Dispersibility-Dependent Biodegradation of Graphene Oxide by Myeloperoxidase. *Small* **2015**, *11*, 3985-3994, doi:10.1002/smll.201500038.
22. Fadeel, B.; Bussy, C.; Merino, S.; Vazquez, E.; Flahaut, E.; Mouchet, F.; Evariste, L.; Gauthier, L.; Koivisto, A.J.; Vogel, U.; et al. Safety Assessment of Graphene-Based Materials: Focus on Human Health and the Environment. *Acs Nano* **2018**, *12*, 10582-10620, doi:10.1021/acsnano.8b04758.

23. Chen, Y.; Zhang, B.; Liu, G.; Zhuang, X.; Kang, E.-T. Graphene and its derivatives: switching ON and OFF. *Chem Soc Rev* **2012**, *41*, 4688-4707, doi:10.1039/C2CS35043B
24. Kuilla, T.; Bhadra, S.; Yao, D.; Kim, N.H.; Bose, S.; Lee, J.H. Recent advances in graphene based polymer composites. *Prog. Polym. Sci.* **2010**, *35*, 1350-1375, doi:https://doi.org/10.1016/j.progpolymsci.2010.07.005.
25. Shao, Y.; Wang, J.; Wu, H.; Liu, J.; Aksay, I.A.; Lin, Y. Graphene based electrochemical sensors and biosensors: a review. *Electroanal* **2010**, *22*, 1027-1036, doi:https://doi.org/10.1002/elan.200900571.
26. Singh, V.; Joung, D.; Zhai, L.; Das, S.; Khondaker, S.I.; Seal, S. Graphene based materials: past, present and future. *Prog. Mat. Sci.* **2011**, *56*, 1178-1271, doi:https://doi.org/10.1016/j.pmatsci.2011.03.003.
27. Tang, B.; Hu, G. Two kinds of graphene-based composites for photoanode applying in dye-sensitized solar cell. *J. Power Sources* **2012**, *220*, 95-102, doi:https://doi.org/10.1016/j.jpowsour.2012.07.093.
28. Goncalves, C.; Goncalves, I.C.; Magalhaes, F.D.; Pinto, A.M. Poly(lactic acid) Composites Containing Carbon-Based Nanomaterials: A Review. *Polymers-Basel* **2017**, *9*, doi:ARTN 26910.3390/polym9070269.
29. Pinto, A.M.; Cabral, J.; Tanaka, D.A.P.; Mendes, A.M.; Magalhaes, F.D. Effect of incorporation of graphene oxide and graphene nanoplatelets on mechanical and gas permeability properties of poly(lactic acid) films. *Polym Int* **2013**, *62*, 33-40, doi:10.1002/pi.4290.
30. Pinto, A.M.; Goncalves, C.; Goncalves, I.C.; Magalhaes, F.D. Effect of biodegradation on thermo-mechanical properties and biocompatibility of poly(lactic acid)/graphene nanoplatelets composites. *Eur Polym J* **2016**, *85*, 431-444, doi:10.1016/j.eurpolymj.2016.10.046.
31. Vieira, A.P., V.C.; Pinto, A.; Magalhães, F.D.; . Viscoplastic model analysis about the influence of graphene reinforcement in poly (lactic acid) time-dependent mechanical behaviour. *International Journal of Automotive Composites 1*, 244-257.
32. Xuequan Zhang, Y.F., Peng Lv, Yongtao Shen, Wei Feng. Enhanced Reversible Photoswitching of Azobenzene-Functionalized Graphene Oxide Hybrids. *Langmuir* **2010**, *26*, 18508-18511, doi:https://doi.org/10.1021/la1037537.
33. Dreyer, D.R.; Park, S.; Bielawski, C.W.; Ruoff, R.S. The chemistry of graphene oxide. *Chem. Soc. Rev.* **2010**, *39*, 228-240, doi:10.1039/B917103G
34. Erwin Peng, E.S.G.C., Prashant Chandrasekharan, Chang‐Tong Yang, Jun Ding, Kai‐Hsiang Chuang, Jun Min Xue. Synthesis of Manganese Ferrite/Graphene Oxide Nanocomposites for Biomedical Applications. *Small* **2012**, *8*, 3620-3630, doi:10.1002/smll.201201427.
35. Huang, H.; Li, Z.; She, J.; Wang, W. Oxygen density dependent band gap of reduced graphene oxide. *J. App. Phys.* **2012**, *111*, 054317, doi:https://doi.org/10.1063/1.3694665.
36. Shang, J.; Ma, L.; Li, J.; Ai, W.; Yu, T.; Gurzadyan, G.G. The origin of fluorescence from graphene oxide. *Sci. Rep.* **2012**, *2*, 792, doi:https://doi.org/10.1038/srep00792.
37. Borges, I.; Henriques, P.C.; Gomes, R.N.; Pinto, A.M.; Pestana, M.; Magalhaes, F.D.; Goncalves, I.C. Exposure of Smaller and Oxidized Graphene on Polyurethane Surface Improves Its Antimicrobial Performance (vol 10, 349, 2020). *Nanomaterials-Basel* **2020**, *10*, doi:ARTN 147010.3390/nano10081470.
38. Gomes, R.N.; Borges, I.; Pereira, A.T.; Maia, A.E.; Pestana, M.; Magalhaes, F.D.; Pinto, A.M.; Goncalves, I.C. Antimicrobial graphene nanoplatelets coatings for silicone catheters. *Carbon* **2018**, *139*, 635-647, doi:10.1016/j.carbon.2018.06.044.
39. Henriques, P.C.; Borges, I.; Pinto, A.M.; Magalhaes, F.D.; Goncalves, I.C. Fabrication and antimicrobial performance of surfaces integrating graphene-based materials. *Carbon* **2018**, *132*, 709-732, doi:10.1016/j.carbon.2018.02.027.
40. Shi, D. *Nanoscience in biomedicine*; Springer Science & Business Media: 2010.
41. Guo, M.; Huang, J.; Deng, Y.; Shen, H.; Ma, Y.; Zhang, M.; Zhu, A.; Li, Y.; Hui, H.; Wang, Y. pH‐responsive cyanine‐grafted graphene oxide for fluorescence resonance energy transfer‐enhanced photothermal therapy. *Adv. Funct. Mat.* **2014**, *25*, 59-67, doi:https://doi.org/10.1002/adfm.201402762.

42. Ma, X.; Tao, H.; Yang, K.; Feng, L.; Cheng, L.; Shi, X.; Li, Y.; Guo, L.; Liu, Z. A functionalized graphene oxide-iron oxide nanocomposite for magnetically targeted drug delivery, photothermal therapy, and magnetic resonance imaging. *Nano Res.* **2012**, *5*, 199-212, doi:10.1007/s12274-012-0200-y
43. Sahu, A.; Choi, W.I.; Lee, J.H.; Tae, G. Graphene oxide mediated delivery of methylene blue for combined photodynamic and photothermal therapy. *Biomaterials* **2013**, *34*, 6239-6248, doi:https://doi.org/10.1016/j.biomaterials.2013.04.066.
44. Thapa, R.K.; Soe, Z.C.; Ou, W.; Poudel, K.; Jeong, J.-H.; Jin, S.G.; Ku, S.K.; Choi, H.-G.; Lee, Y.M.; Yong, C.S. Palladium nanoparticle-decorated 2-D graphene oxide for effective photodynamic and photothermal therapy of prostate solid tumors. *Colloids Surf. B.* **2018**, *169*, 429-437, doi:https://doi.org/10.1016/j.colsurfb.2018.05.051.
45. Yang, H.-W.; Lu, Y.-J.; Lin, K.-J.; Hsu, S.-C.; Huang, C.-Y.; She, S.-H.; Liu, H.-L.; Lin, C.-W.; Xiao, M.-C.; Wey, S.-P. EGRF conjugated PEGylated nanographene oxide for targeted chemotherapy and photothermal therapy. *Biomaterials* **2013**, *34*, 7204-7214, doi:https://doi.org/10.1016/j.biomaterials.2013.06.007.
46. Sharma, M. Transdermal and intravenous nano drug delivery systems: present and future. In *Applications of targeted nano drugs and delivery systems*; Elsevier: 2019; pp. 499-550.
47. Zempsky, W.T.J.P. Alternative routes of drug administration—advantages and disadvantages (subject review). *Pedriactics* **1998**, *101*, 730-731, doi:https://doi.org/10.1542/peds.101.4.730.
48. Khan, M.S.; Abdelhamid, H.N.; Wu, H.-F. Near infrared (NIR) laser mediated surface activation of graphene oxide nanoflakes for efficient antibacterial, antifungal and wound healing treatment. *Colloids Surf. B.* **2015**, *127*, 281-291, doi:https://doi.org/10.1016/j.colsurfb.2014.12.049.
49. Dubey, N.; Mishra, S.; Mukerjee, A.; Singh, A. Graphene conjugated usnic acid nano-formulation for the treatment of topical fungal infection. *J. Pharm. Pharm. Sci.* **2020**, *12*, 47-53, doi:: http://dx.doi.org/10.22159/ijpps.2020v12i5.34724.
50. Luo, S.; Jin, S.; Yang, T.; Wu, B.; Xu, C.; Luo, L.; Chen, Y. Sustained release of tulobuterol from graphene oxide laden hydrogel to manage asthma. *J. Biomater. Sci. Polym. Ed.* **2020**, 1-12, doi:https://doi.org/10.1080/09205063.2020.1849921.
51. Marcano, D.C.; Kosynkin, D.V.; Berlin, J.M.; Sinitskii, A.; Sun, Z.; Slesarev, A.; Alemany, L.B.; Lu, W.; Tour, J.M. Improved synthesis of graphene oxide. *ACS Nano* **2010**, *4*, 4806-4814, doi:https://doi.org/10.1021/nn1006368.
52. Costa-Almeida, R.; Bogas, D.; Fernandes, J.R.; Timochenco, L.; Silva, F.A.; Meneses, J.; Gonçalves, I.C.; Magalhães, F.D.; Pinto, A.M. Near-Infrared Radiation-Based Mild Photohyperthermia Therapy of Non-Melanoma Skin Cancer with PEGylated Reduced Nanographene Oxide. *Polymers* **2020**, *12*, 1840, doi:https://doi.org/10.3390/polym12081840.
53. Liang, A.; Jiang, X.; Hong, X.; Jiang, Y.; Shao, Z.; Zhu, D. Recent developments concerning the dispersion methods and mechanisms of graphene. *Coatings* **2018**, *8*, 33, doi:https://doi.org/10.3390/coatings8010033.
54. Salopek, B.; Krasic, D.; Filipovic, S. Measurement and application of zeta-potential. *RGN zbornik* **1992**, *4*, 147.
55. Rodrigues, A.F.; Newman, L.; Lozano, N.; Mukherjee, S.P.; Fadeel, B.; Bussy, C.; Kostarelos, K.J.D.M. A blueprint for the synthesis and characterisation of thin graphene oxide with controlled lateral dimensions for biomedicine. *Carbon* **2018**, *99*, 318-329, doi:https://doi.org/10.1016/j.carbon.2015.11.076.
56. Uran, S.; Alhani, A.; Silva, C. Study of ultraviolet-visible light absorbance of exfoliated graphite forms. *AIP adv.* **2017**, *7*, 035323, doi:https://doi.org/10.1063/1.4979607.
57. Lademann, J.; Richter, H.; Schanzer, S.; Knorr, F.; Meinke, M.; Sterry, W.; Patzelt, A. Penetration and storage of particles in human skin: perspectives and safety aspects. *Eur J Pharm Biopharm* **2011**, *77*, 465-468, doi:https://doi.org/10.1016/j.ejpb.2010.10.015.
58. Gupta, R.; Debbaneh, M.; Butler, D.; Huynh, M.; Levin, E.; Leon, A.; Koo, J.; Liao, W. The Goeckerman Regimen for the Treatment of Moderate to Severe Psoriasis. *Jove-J Vis Exp* **2013**, doi:ARTN e5050910.3791/50509.
59. Costa-Almeida, R.; Bogas, D.; Fernandes, J.R.; Timochenco, L.; Silva, F.; Meneses, J.; Goncalves, I.C.; Magalhaes, F.D.; Pinto, A.M. Near-Infrared Radiation-Based Mild Photohyperthermia Therapy of Non-Melanoma Skin Cancer with PEGylated Reduced Nanographene Oxide. *Polymers (Basel)* **2020**, *12*, doi:10.3390/polym12081840.

 doi:10.20944/preprints202103.0550.v1

60. Daniyal, M.; Liu, B.; Wang, W. Comprehensive Review on Graphene Oxide for Use in Drug Delivery System. *Curr Med Chem* **2020**, *27*, 3665-3685, doi:10.2174/1381612825666190201129629O.